applied sciences

MDPI

Article

Bearing Capacity of a Concrete Grouting Pad on the Working Surface of a Highway Tunnel Shaft

Tengfei Fang [1], Zongzhi Zhao [2,3], Jianxun Chen [1,*], Yanbin Luo [1], Weiwei Liu [1], Dong Li [2], Ruibin Yu [2] and Jian Li [2]

[1] School of Highway, Chang'an University, Xi'an 710064, China; 2022021048@chd.edu.cn (T.F.)
[2] CCCC Central-South Engineering Co., Ltd., Changsha 410116, China
[3] CCCC First Highway Engineering Company, Beijing 100024, China
* Correspondence: chenjx1969@chd.edu.cn

Abstract: A grouting pad is the key structure for the construction of water inrush grouting on the shaft working surface. Previous methods of calculating the bearing capacity have limitations due to a lack of understanding of the failure mode. To investigate the bearing capacity of a concrete grouting pad on the working surface of a shaft, this paper establishes a mechanical model for the punching shear failure of a grouting pad under symmetrical loading conditions. A unified solution for the bearing capacity is derived, and the influence of parameters is discussed. In addition, a new method for designing the plastic limit thickness is proposed based on this research. The results show that the reason for the grouting pads' punching shear failure resulted from the formation of peripheral grouting holes "weak ring" caused by the reduction of the bearing capacity. When the thickness of B_0 remains constant, the bearing capacity q_u of the grouting pad is inversely proportional to the ratio of the diameter and the area of the bottom load. Therefore, following the method of "dividing, interval, and jumping holes" during grouting construction is recommended. The greater the thickness of the grouting pad, the greater the bearing capacity q_u will be. When the grouting pad diameter is $2r_2$ and the thickness B_0 is constant, the bearing capacity q_u increases with the material tensile strength f_t. When designing grouting pads, following the principles of "large thickness, uniform strength theory, high strength materials" will improve bearing performance. The findings have been implemented in the design of the grouting pad thickness for the Tianshan Shengli Tunnel shaft project, which can successfully solve the problem of frequent cracking caused by the weak bearing capacity of a grouting pad. The findings can provide a theoretical basis and reference for the design and construction of grouting pads in a highway tunnel shaft.

Keywords: grouting pad; punching shear failure; unified strength theory; bearing capacity; thickness design

Citation: Fang, T.; Zhao, Z.; Chen, J.; Luo, Y.; Liu, W.; Li, D.; Yu, R.; Li, J. Bearing Capacity of a Concrete Grouting Pad on the Working Surface of a Highway Tunnel Shaft. *Appl. Sci.* **2024**, *14*, 2933. https://doi.org/10.3390/app14072933

Academic Editor: Tiago Miranda

Received: 29 February 2024
Revised: 27 March 2024
Accepted: 28 March 2024
Published: 30 March 2024

1. Introduction

Mountainous terrain is steep, and tunnels have become the main way to break down traffic barriers [1–4]. To meet the ventilation requirements for construction and operation, constructing deep and large shafts is the optimal choice for extra-long highway tunnels [5,6]. As shaft sinking depth increases, the problem of water gushing into the fractured surrounding rock during the construction period is highlighted, and the adoption of scientific and rational grouting measures plays an important role in the prevention and control of water damage [7]. To achieve this, it is particularly critical to clarify the bearing capacity of a shaft grouting pad in order to reasonably determine the thickness.

Many scholars have focused on the issue of grouting pads in wellbore workings. Chai et al. [8] and Li et al. [9] have both adopted the elastomechanical method to design the thickness of a high-pressure deep-hole pregrouting pad in the treatment of water inrush in a coal mine shaft of water-enriched geology. Wang and Pan et al. [10,11] gave empirical formulae for the thickness of a grouting pad for the sudden water flooding project of a vertical

iron ore and coal mine shaft, taking into account the stratigraphic–hydrological conditions of the shaft site area. Qian [12] and Zhai et al. [13] proposed an empirical formula applicable to the thickness of a grouting pad in a 1# sub-shaft aiming at the inrush of water in a Tianxing iron mine. Zheng et al. [14] proposed a formula for calculating the thickness of a two-stage underwater cast-in-place grouting pad based on the geological and construction conditions for a mine in the excavation of a sub-shaft cavern in the Nanli Iron Mine. Ge et al. [15] predicted the grouting volume of a gushing shaft using an adaptive fuzzy neural system and multi-regression methods. Hancock et al. [16], who analysed the gushing water problem in the construction of a tin mine shaft in Australia, believed that the adoption of reasonable grouting in the construction of a shaft has positive significance for the construction period and construction cost control. Bukowski [17] established a gushing water hazard risk assessment method for gushing water hazards to determine the potential factors for the occurrence of gushing water in coal mine shafts. Han et al. [18] analysed the mechanisms of water gushing in a shaft constructed by the freezing method in coal mines in western China, constructed a risk assessment model of water gushing, and proposed the parameters of a grouting pad, which can be used as a reference for the prevention and control of water gushing in a shaft constructed by the anti-freezing method. Kipko [19] illustrated the engineering practical experience of successful water plugging by surface pumping grouting with an example from the flooded accident of the abandoned shafts of a coal mine in the former Czechoslovakian area. Xu et al. [20] studied the technology of the simultaneous operation technique of the mechanical shaft boring construction and surface deep-hole grouting for vertical shafts in deep alluvial formations, proposing safety measures that can be implemented.

The above research enriches the theory and technology of the prevention and control of water inrush hazards during a shaft construction period and provides a necessary basis for future work. However, there are some limitations and shortcomings. First, most of the research objects pay attention to a coal mine shaft, while there is little literature related to the grouting of the working surface of a highway tunnel shaft, and the shaft diameter is often 1–3 m larger than that of a coal mine shaft. Therefore, the mechanical model of a grouting pad belongs to the problem of plastic mechanics of a thin plate [21], and the calculation formula obtained by combining the plane common point force with experience is unreasonable. Secondly, there is a bias in the understanding of the failure mode of a grouting pad. The author has observed in the field that the failure mode of a grouting pad was a punching shear failure, guided by cracking along the peripheral grouting holes, rather than a punching shear failure with overall cracking at the bottom [22]. Thirdly, the treatment of the load on a grouting pad deviates from the actual situation in the field. Even in the case of poorly fractured rock, the peripheral high-pressure grouting holes generate a back pressure that is difficult to apply to the entire bottom of a grouting pad [23]. Therefore, the load range of a grouting pad should be simplified to the vicinity of the grouting holes.

Consequently, this paper analyses the failure mode of a grouting pad and establishes a mechanical model under symmetrical loading. Firstly, a unified yield criterion is introduced, and the plastic limit load of grouting pad punching shear failure is derived. Secondly, the rationality of the understanding is verified, and the influence of plastic ultimate load parameters is discussed. Finally, a design method for the plastic limit of slurry cushion thickness is proposed. The research results have been applied to the design of grouting pads for well 2-2 of the Tianshan Shengli Tunnel, one of the longest highway tunnels in the world. This method solves the problem of frequent cracking caused by insufficient bearing capacity in the elastic design of grouting pads. The results of the study can provide a reference for the design and construction of grouting pads in similar shaft projects.

2. Grouting Pad Failure Mode

Compared with mine shafts, highway tunnel shafts have larger diameters, usually ranging from 7 to 10.5 m. The grouting pad thickness typically ranges from 2 to 4 m, resulting in a thickness-to-diameter ratio close to 0.2. Therefore, it is treated as a circular

thin plate problem [21]. Based on the analysis of failure modes in simply supported circular plates, it is observed that tangential bending moments act along the radial direction, while radial bending moments act annularly along different coefficients multiplied by the radius (less than 1) [24]. Tangential bending moments generate radial cracks, while radial bending moments generate annular cracks.

Based on the above discussion, the failure mode of a shaft grouting pad is analysed. Regarding the grouting pad on the working surface of the shaft, the grouting holes are generally arranged along the periphery of the grouting pad at a certain distance from the circumferential spacing, and all the grouting holes are used for high-pressure grouting on the rock body of the working surface. After closing the grouting valve, the load acting on the bottom surface of the grouting pad consists of two parts, one of which is the pressurised water of the working surface, and the other one is the lifting force generated by the diffusion of the grout from the grouting holes [25]. Both forces act in the same direction on the bottom of the grouting pad, as shown in Figure 1.

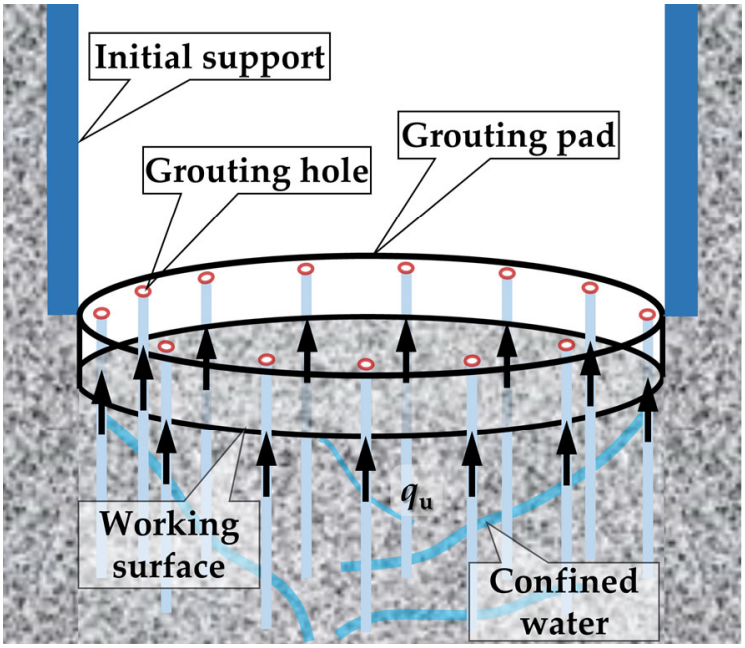

Figure 1. The force on the shaft grouting pad.

To facilitate the installation of the orifice pipe, the grouting hole must pass through the full thickness of the grouting pad during the hole forming process. This results in the formation of a ring hole "weak ring" around the grouting pad. It is worth noting that this "weak ring" is caused by the grouting hole cracking at a certain distance around the grouting pad. This "weak ring" provides a stress concentration area for cracks caused by tangential and radial bending moments [26]. However, its ring is more conducive to the propagation and extension of circumferential cracks. During grouting construction, it is important to balance the peripheral pressure in the relative direction of the grouting pad to prevent ring cracking on one side of the pad. It is also important to consider the limited ability of the grout to spread after closing the grouting valve. This can often result in punching shear failure within a certain range from the mouth of the hole, as shown in Figure 2.

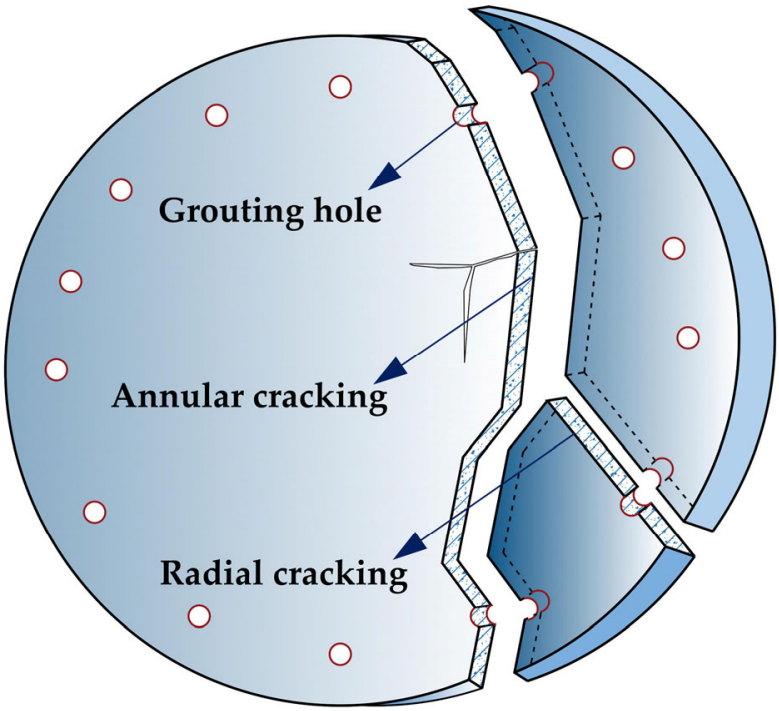

Figure 2. Cracking and failure of the grouting pad.

3. Deduction of Plastic Ultimate Load of the Grouting Pad

3.1. Double-Shear Unified Yield Criterion

The double-shear unified yield criterion [27] can be given as Equation (1):

$$\left.\begin{aligned} F &= \sigma_1 - \tfrac{1}{1+b}(b\sigma_2 + \sigma_3) = \sigma_t\sigma_2 \le (\sigma_1 + \sigma_3)/2 \\ F' &= \tfrac{1}{1+b}(\sigma_1 + b\sigma_2) - \sigma_3 = \sigma_t\sigma_2 \ge (\sigma_1 + \sigma_3)/2 \end{aligned}\right\} \quad (1)$$

where F and F' are yield functions; σ_1–σ_3 is the first, middle, third principal stress, MPa; b is the influence coefficient of intermediate principal stress on the strength of the material; σ_t is the tensile strength of the material, MPa.

For axisymmetric circular plates, the double-shear unified yield criterion is used to express plastic yielding in terms of bending moments. This criterion is described in the tangential moment–radial moment (M_θ–M_r) plane, as shown in Figure 3. To account for the unknown direction of the principal stress during plastic deformation, Equation (1) is decomposed into six expressions. When the limit bending moment is satisfied by any of the expressions, it is considered that the point has entered a plastic state. This can be converted into a double-shear unified yield condition expressed by generalised stress [28], and it can be given as Equation (2):

$$\begin{aligned} &\max\left(\left|M_r - \tfrac{b}{1+b}M_\theta\right|, \left|M_r - \tfrac{1}{1+b}M_\theta\right|, \tfrac{1}{1+b}|bMr + M_\theta|,\right. \\ &\left.\left|\tfrac{1}{1+b}M_r - M_\theta\right|, \tfrac{1}{1+b}|M_r + bM_\theta|, \left|\tfrac{b}{1+b}M_r - M_\theta\right|\right) \end{aligned} \quad (2)$$

where M_r is the radial bending moment, kN/m; M_θ is the tangential bending moment, kN/m.

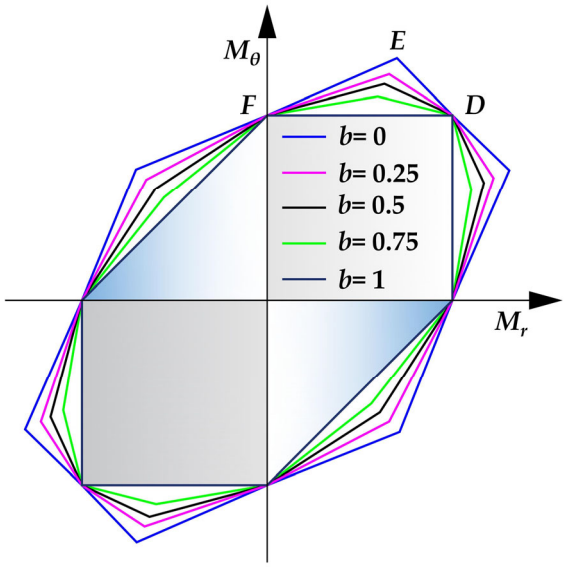

Figure 3. Double-shear uniform yield line for a circular plate.

3.2. Computational Model and Solution Method

According to the above analysis of the failure mode of the grouting pad, the solution to the punching shear bearing capacity of the grouting pad involves the problem of plastic deformation of the circular plate under the action of a uniform circumferential load. The boundary constraint conditions are equivalent to a simple support due to the fact that the grouting pad and the initial support structure were not poured simultaneously. Prior to conducting the plastic limit analysis, it is essential to make the following assumptions regarding deformation and stress:

1. The vertical line of the neutral surface of the plate is unchanged in length and state before and after deformation;
2. The deflection of the neutral plane is much smaller than the plate thickness;
3. The normal stress σ_z in the neutral plane is much smaller than other stress components and can be neglected.

The computational model and micro-hexahedral unit forces are established, as shown in Figures 4 and 5.

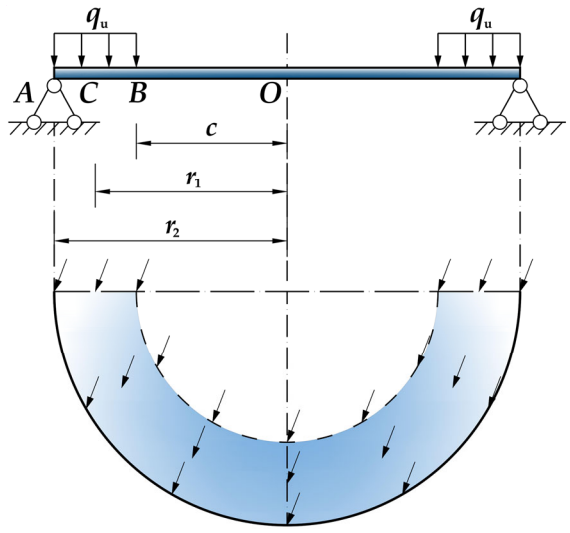

Figure 4. Mechanical calculation model.

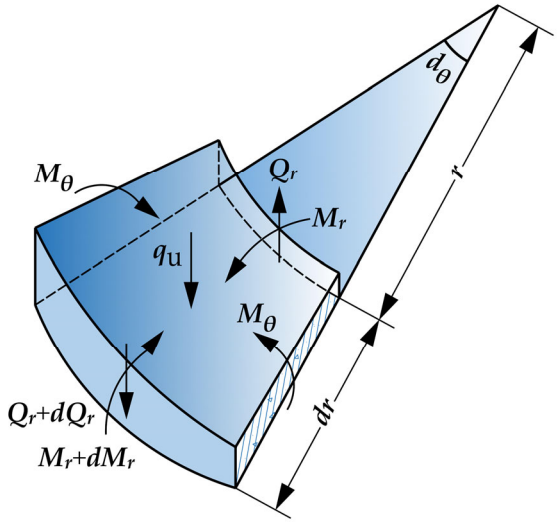

Figure 5. Micro-hexahedral unit.

As shown in Figure 5, according to the force equilibrium of the plate microelement under axisymmetric load, it can be given as Equation (3):

$$\frac{d(rM_r)}{dr} = M_\theta + rQ_r \tag{3}$$

where Q_r is the shear force acting on the unit, kN; r is the radius of the circular plate, m; dr is the micro-hexahedral element radius; dM_r is the micro-hexahedral element radial bending moment.

As shown in Figures 4 and 5, because of the section of the yield condition and the discontinuity of the plate load distribution, resulting in (3) type differential equation solution process needs to be based on different boundary conditions to select the corresponding yield condition, and thus the partition solution idea, to a point on the plate bending moment C as a reference point, set it is located in the E yield point, combined with the Figures 3 and 4 to discuss the solution.

3.3. Equilibrium Equations and Yield Conditions

3.3.1. Centre and Simply Supported Boundary

At the centre of the circular plate r = 0, the boundary condition satisfies $M_r|_{r=0} = M_\theta|_{r=0} \neq 0$, and the yield condition satisfies the D point in Figure 3. At the edge of the circular plate $r = r_2$, the boundary condition satisfies $M_r|_{r=r_2} = 0$, and the yield condition satisfies the F point in Figure 3. Therefore, from the $r = -r_2$ to $r = r_2$ position, the yield condition satisfies the DE, EF segments in Figure 3, and it can be given as Equation (4):

$$\left.\begin{array}{l} DE: \frac{b}{1+b}M_r + \frac{b}{1+b}M_\theta = M_\mathrm{p} \\ EF: M_\theta - \frac{b}{1+b}M_r = M_\mathrm{p} \end{array}\right\} \tag{4}$$

where M_p is the cross-sectional ultimate bending moment, kN/m.

3.3.2. Point C Is in the Range of the Simply Supported Plate AB

When point C is within the range of simply supported plate AB, the AO section of the axisymmetric circular plate is divided into three sections: AC, CO, and BO. The equi-

librium equations are listed, respectively, and the yield condition is selected according to Formula (4), given as Equation (5):

$$\left.\begin{array}{ll} OB \text{ segment}: r\frac{dMr}{dr} = (1+b)(M_{\mathrm{p}} - M_r) & DE \text{ segment yield line} \\ BC \text{ segment}: r\frac{dMr}{dr} = (1+b)(M_{\mathrm{p}} - M_r) - \frac{q_{\mathrm{u}}}{2}(r^2 - c^2) & DE \text{ segment yield line} \\ CA \text{ segment}: r\frac{dMr}{dr} = (1+b)(M_{\mathrm{p}} - M_r) - \frac{q_{\mathrm{u}}}{2}(r^2 - c^2) & EF \text{ segment yield line} \end{array}\right\} \quad (5)$$

where c is the grouting diffusion boundary value, m; q_{u} is the ultimate bearing capacity of a circular plate, MPa.

3.3.3. Point C Is in the Range of the Simply Supported Plate BO

According to the double-shear unified yield criterion, the equilibrium equations can be listed, and it can be given as Equation (6):

$$BO \text{ scope}: r\frac{dMr}{dr} = (1+b)(M_{\mathrm{p}} - M_r) \quad DE \text{ segment yield line} \quad (6)$$

Meanwhile, when point C is within the range of the simply supported plate BO, it also satisfies Equation (3) and $Q_r = 0$. Solving Equation (3) yields $M_r = M_\theta$, and solving Equation (6) yields $2M_r = M_\theta$. These results contradict each other, indicating that point C cannot be within the range of the simply supported plate BO when it is at the E yield point.

3.4. Boundary Conditions

The boundary conditions primarily examine the existence and continuity of the values of the four points O, B, C, and A, where point O satisfies $M_r|_{r=0} = M_\theta|_{r=0} \neq 0$, points B and C satisfy the continuity, and point C satisfies $2M_r = M_\theta$ from the analysis in the previous section.

3.5. Bearing Capacity Solution

Equations (4) and (5) will be used to substitute into the boundary conditions, resulting in the final solution for the grouting pad bearing capacity, given as Equation (7):

$$q_{\mathrm{u}} = \frac{(2b^2 + 6 + 8b)M_{\mathrm{p}}}{(2+b)\left[2c^2(c/r_1)^{1+b} - (3+b)c^2 + r_1^2(b+1)\right]} \quad (7)$$

where r_1 is the calculation reference radius, m.

Parameter r_1 conforms to the non-linear equation and can be given as Equation (8):

$$\begin{array}{l} 2(1+b)(3+2b)c^2(c/r_1)^{1+b} + (2b^3 + 6b^2 + 4b)r_1^2 \\ +(b^2 + 4b + 3)\left[r_2^2 - (3+2b)c^2\right](r_2/r_1)^{1/(1+b)} - \\ (2b^2 + 7b + 6)\left[(1+b)r_1^2 - (3+b)c^2\right](r_2/r_1)^{1/(1+b)} \\ -(4b^2 + 14b + 12)c^2(c/r_1)^{1+b}(r_2/r_1)^{1/1+b} = 0 \end{array} \quad (8)$$

Parameter r_1 can be solved by Newton's iterative method, with $r_1 = x$, taking the initial value of x_0, defining the accuracy e^*, and constructing the iterative function and equation. It can be given as Equation (9):

$$\left.\begin{array}{l} x = x_0 - f(x)/f'(x) \\ |(x - x_0)/x| \leq e^* \end{array}\right\} \quad (9)$$

where $f(x)$ is the iterative function; $f'(x)$ is the derivative of the iterative function.

In order to further illustrate the steps of Newton's iterative method for solving r_1, a specific algorithm flowchart is provided. The algorithm can be solved using 2016 Excel software, as shown in Figure 6.

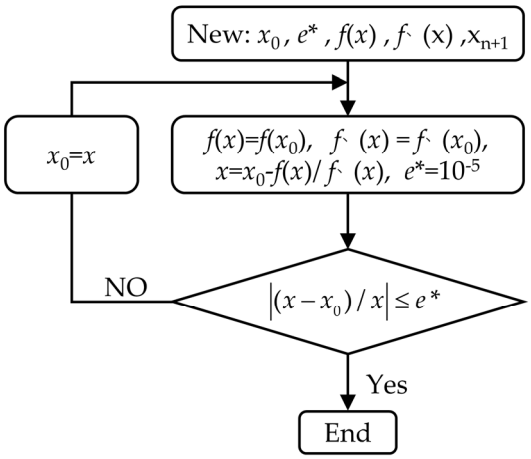

Figure 6. Newton's iterative algorithm process.

4. Parameter Sensitivity Analysis

4.1. Verification of the Reasonableness of the Solution

Figure 3 shows that the uniform strength yield criterion can be degraded to the typical properties of the other yield criteria depending on the values of b. The Tresca yield criterion is commonly used in plastic structural analysis when $b = 0$, while the double-shear unity yield criterion is used when $b = 1$. When $b = 0.5$, it approximates the Mises yield [28]. Due to space limitations, this paper compares the solution of the Tresca yield criterion with $b = 0$ by substituting it into Equations (7) and (8).

The derivation of the Tresca yield criterion q_u for the circular plate AB, ranging from $c \le r \le r_2$, satisfies $M_\theta \ge M_r \ge 0$ and $M_p = M_\theta$. Substituting these values into Equation (3) gives Equation (10):

$$M_r = M_p + \frac{q_u}{2}(c^2 - r^2/3) + S_1/r \tag{10}$$

For the round board BO range, the Tresca yield criterion satisfies $M_p = M_\theta$, and because of $M_r = M_\theta$, so $M_p = M_r$, according to $r = c$ solution S_1, and substituting $(M_r)_{r=r_2} = 0$ into Equation (10), it can be given as Equation (11):

$$q_u = \frac{6M_p}{r_2^2 - 3c^2 + 2c^3/r_2} \tag{11}$$

Equation (11) happens to be a special case of Equation (7) when $b = 0$, which shows that the unified solution in this paper is reasonable and has good extensions.

4.2. Effect of b on Load-Bearing Capacity q_u

Using $c = 3$ m, $r_2 = 5.5$ m, and $M_p = 16.41$ MPa, Figure 7 illustrates the impact of the b value on q_u. The Tresca yielding criterion solution is a special case of this paper when $b = 0$, while the Mises yielding criterion solution is a special case of this paper when $b = 0.5$. This demonstrates the rationality of the unified solution presented in this paper. As the value of b increases, q_u shows a tendency to decrease and then increase. It reaches a minimum value at $b = 0.4$, which is close to 5.03×10^3 kN/m^3, and a maximum value at $b = 1$, which is close to 8.04×10^3 kN/m^3. The increase in the q_u value of 6.7% for $b = 1$ compared to $b = 0$ and 59.8% compared to $b = 0.5$ suggests that the double-shear unified strength yield criterion is more capable of utilising the potential of material strength compared to the Tresca and Mises yield criterion.

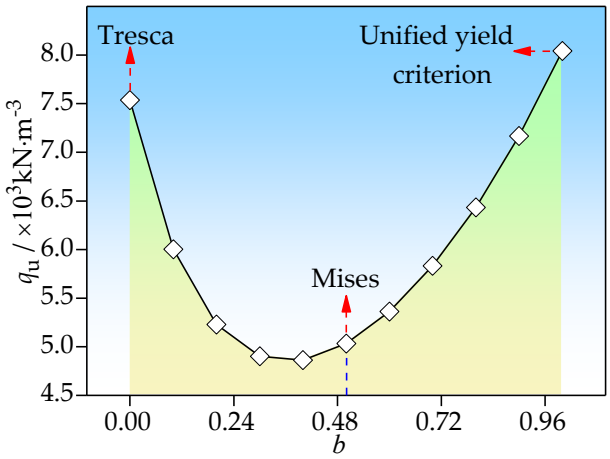

Figure 7. Parameter q_u–b relationship curve.

4.3. Effect of Shaft Radius r_2 on Bearing Capacity q_u

Figure 8 illustrates the impact of the effect of shaft radius r_2 on q_u under different b value conditions. The results indicate that q_u decreases as the r_2/c value increases, while the b value remains constant. The bearing capacity of the grouting pad increases with an increase in the b value for a given value of r_2/c. Assuming a constant thickness, the bearing capacity of the grouting pad is inversely proportional to the ratio of the diameter to the area of the bottom loaded area. When the value of b is set to 1, the grouting pad q_u increases by 15% to 87% compared to when b is set to 0.5. Similarly, when b is set to 1, q_u increases by 0.5–1.3 times compared to when b is set to 0.75. These results indicate a significant increase in the grouting pad q_u when considering the contribution of the middle principal stress. When b is set to 0.5 and 1, q_u increases by 15–87%. When b is taken as 0.75 and 1, the q_u increases by 0.5–1.3 times. After considering the contribution of medium principal stress, the q_u of the grouting pad significantly increased. Specifically regarding construction practice, reflection of the working surface high-pressure grouting holes should be placed at the edge of the grouting pad to reflect the working surface. The grouting length should be reasonably controlled to avoid high-pressure grouting in the surrounding holes. It is important to reduce the diffusion area of the grouting pad pulp at the bottom to minimise the possibility of punching shear failure. Therefore, the construction of grouting should follow the principle of "subdivision, time interval, and jump hole".

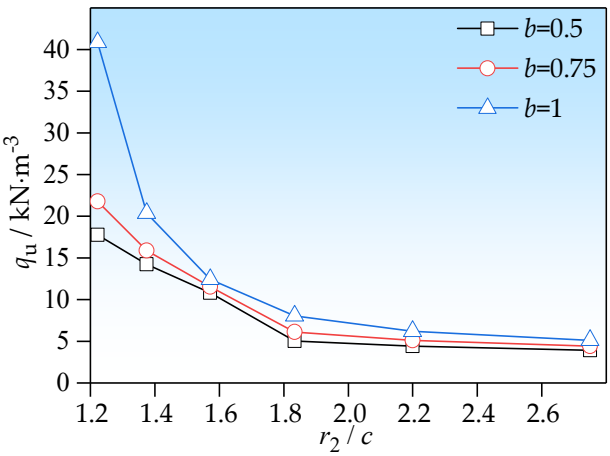

Figure 8. Effect of the r_2/c ratio on q_u.

When $c = 3$ and $b = 1$, we analysed the effect of r_2/r_1 on the bearing capacity q_u. Figure 9 shows a non-linear relationship between r_2/r_1 and q_u. As r_2/r_1 increases, q_u first decreases

slowly, then experiences a sudden increase, and finally decreases again. This means that larger r_2/r_1 ratios do not necessarily result in larger q_u values. Instead, q_u reaches its relative maximum value at a certain ratio of r_2/r_1. This point aims to guide engineering practice by recommending the use of a uniform yield criterion for designing grouting pads. It is important to check whether the r_2/r_1 ratio is close to 1.25 to verify the calculation's reasonableness.

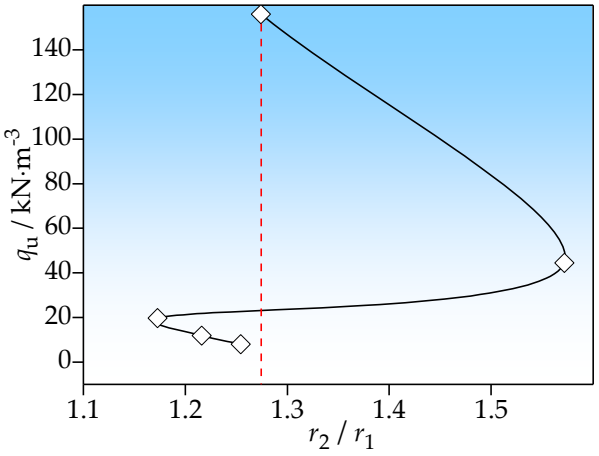

Figure 9. Effect of the value of r_2/r_1 on q_u when b = 1.

The influence of r_2/c on the value of r_1 was calculated using the iterative method, as shown in Figure 10. The value of r_1 exhibits a three-stage trend of decreasing, then increasing, and finally decreasing again as r_2/c increases. When r_2/c is less than 1.375, r_1 is the largest when b = 1 and the smallest when b = 0.5. When r_2/c is between 1.375 and 1.571, the maximum r_1 is obtained when b = 0.75, and the minimum r_1 is obtained when b = 0.5. When r_2/c is greater than 1.833, r_1 is the minimum when b = 1.

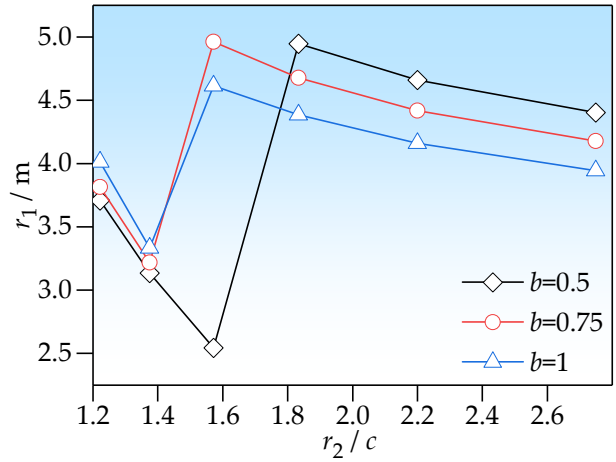

Figure 10. The r_1–r_2/c relationship when b = 1.

4.4. Effect of Section M_p Parameters on Bearing Capacity

The impact of the cross-section M_p parameter on q_u is examined under various b value conditions. The influential parameters of cross-section M_p are grouting pad diameter $2r_2$, thickness B_0, and concrete material tensile strength f_t, respectively, discussing the relationship between each parameter and q_u, as shown in Figures 11–13.

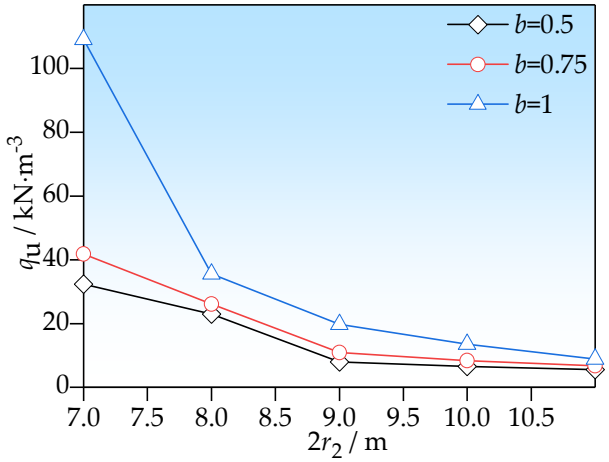

Figure 11. The q_u–$2r_2$ relationship curve.

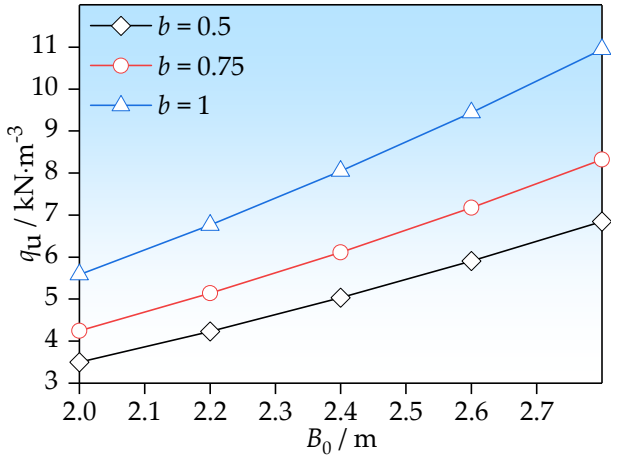

Figure 12. The q_u–B_0 relationship curve.

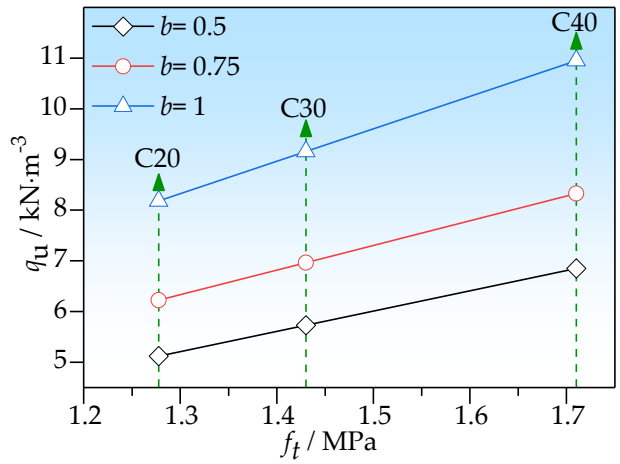

Figure 13. The q_u–f_t relationship curve.

Figure 11 shows that the bearing capacity q_u of the grouting pad decreases as the diameter $2r_2$ increases when the thickness B_0 of the grouting pad is constant, which is consistent with the theory of thin plate failure. Moreover, increasing the value of b for any diameter condition results in a greater bearing capacity q_u of the grouting pad. For a

vertical or 7 m diameter shaft, when $b = 1$, q_u is approximately 2.4–3.3 times greater than when $b = 0.5$ or $b = 0.75$.

Figure 12 shows that the bearing capacity q_u of the grouting pad $2r_2$ increases with the thickness B_0. This indicates that a thicker grouting pad can bear a greater capacity q_u under the same load conditions. Furthermore, the bearing capacity q_u of the grouting pad increases with the value of b for any given thickness condition. For a 2.0 m thick grouting pad, when $b = 1$, q_u increases by 59.8% compared to $b = 0.5$ and 31.5% compared to $b = 0.75$.

Figure 13 shows that the bearing capacity q_u increases with the design value of the tensile strength f_t of the grouting pad concrete material when the diameter of the grouting pad $2r_2$ and the thickness B_0 remain constant. This indicates that under the same load conditions, the bearing capacity q_u is greater with higher tensile strength of the grouting pad concrete material. For example, when $b = 1$, q_u increases by 59.8% compared to $b = 0.5$ and by 31.5% compared to $b = 0.75$. To achieve better bearing performance when designing the grouting pad poured with C20 concrete, following the principles of "large thickness, high-strength materials, and unified strength yield criteria" is recommended.

5. Design Method and Engineering Application of Grouting Pad Thickness

5.1. Design Method of Grouting Pad Thickness

To design the thickness of a flat-bottomed grouting pad, China's coal mine vertical shafts often use the calculation method shown in Equation (12) [29]:

$$B_0 = P_0 r_2 / [\sigma_c] + 0.3 r_2 \tag{12}$$

where B_0 is the thickness of the grouting pad, m; P_0 is the termination pressure of the grouting orifice, MPa; $[\sigma_c]$ is the permissible uniaxial compressive strength of the grouting pad concrete, MPa.

Equation (12) shows that the formula belongs to the elastic design method, which prohibits plastic deformation inside the grouting pad. However, deformation of the grouting pad is allowed to occur during field grouting construction due to the appearance of the plastic region of the grouting pad. Therefore, this paper proposes the design method for the plastic limit of the shaft grouting pad.

Separate the cross-sectional ultimate bending moment M_p variable in Equation (7), which can be given as Equation (13):

$$M_p = \frac{q_u(2+b)\left[2c^2(c/r_1)^{1+b} - (3+b)a^2 + r_1^2(b+1)\right]}{(2b^2+6+8b)} \tag{13}$$

According to the formula for calculating the bending normal stress of a cross-section in material mechanics [30], the ultimate bending moment inside a circular plate can be obtained, given as Equation (14):

$$M_p = \sigma_s W_x = \frac{1}{6}(2r_2)B_0^2\sigma_s = \frac{r_2 B_0^2 \sigma_s}{3} \tag{14}$$

where σ_s takes the design value of tensile strength of the grouting pad, MPa; W_x is the grouting pad section modulus, m^3.

To solve for B_0, substitute Equation (14) into Equation (13), replace the plastic ultimate load q_u with P, and define the safety factor γ; the solution can be given as Equation (15):

$$B_0 = \sqrt{\frac{3P\gamma b(2+b)\left[2c^2(c/r_1)^{1+b} - (3+b)c^2 + r_1^2(b+1)\right]}{r_2(2b^2+6+8b)\sigma_s}} \tag{15}$$

where P is the mean grouting pressure of the working surface and single hole, MPa; γ is the safety coefficient. Considering the importance of the engineering service cycle, it is recommended that the mine shaft γ should be 1.2 and the tunnel shaft γ should be 1.5.

Equation (7) can be used to calculate the bearing capacity of the constructed grouting pad, which guides the grouting construction. Equation (15) is used for the design of grouting pad thickness and material selection based on grouting pressure and water pressure. Both equations ensure a scientific and reasonable grouting of the working surface.

In order to facilitate better implementation by design and construction personnel, a specific design process is given, as shown in Figure 14. Firstly, determine the strength theory b value, shaft radius r_2, grouting diffusion radius c (three parameters), so as to substitute into Formula (8) to calculate the r_1 value and, at the same time, to determine the value of the working surface of the shaft water pressure value p_w and p_{az} to calculate the value of P,as well as concrete material σ_s (f_t) and the safety factor γ. Secondly, the above seven parameters are substituted into Formula (15) to calculate the thickness of the grouting pad B_0. Finally, the site construction is carried out according to the designed thickness of the grouting pad.

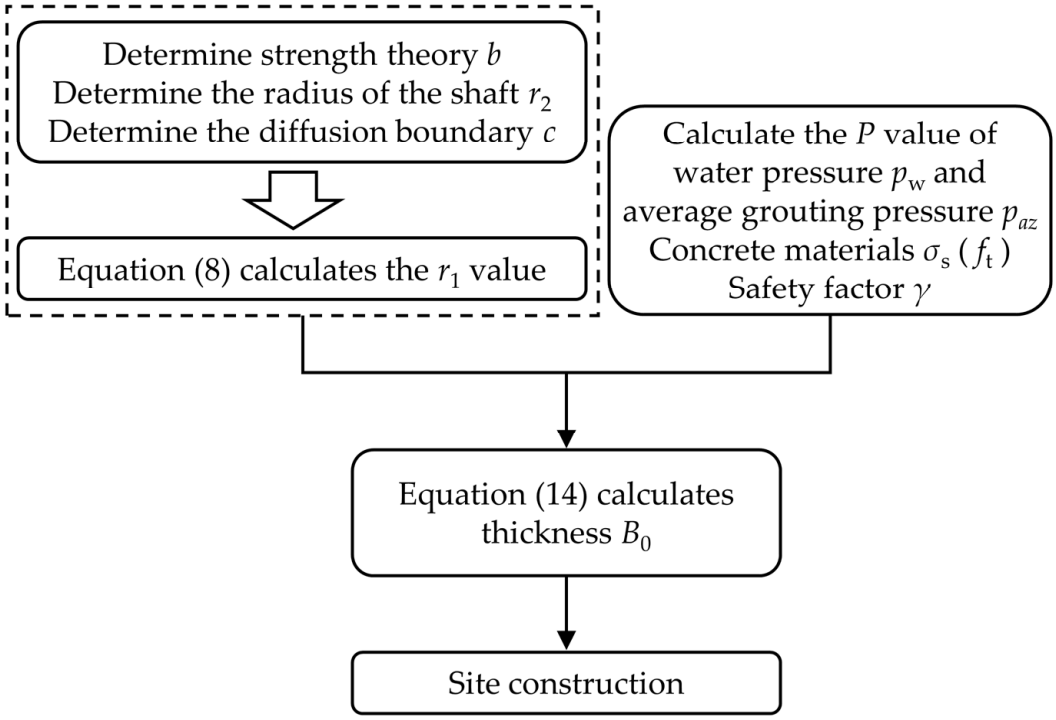

Figure 14. Design flow chart.

5.2. Engineering Applications

5.2.1. Project Overview

The Tianshan Shengli Tunnel is a key project of the Urumqi–Yuli Expressway in China. The tunnel is 22.13 km long, and it is the longest highway tunnel under construction in the world. The tunnel adopts the construction method of "3 main tunnels and 4 shafts". The No. 2-2 shaft has a design diameter of 10.5 m and a depth of 704 m, making it the largest diameter highway tunnel shaft under construction in China. During the construction of the 2-2 shaft, when drilling to the ◎ granite crushing zone, there were many water surges in the working face, and the water surges were as high as 40 m^3/h. During the grouting and water blocking process in the working face, the grouting pads were cut and cracked, affecting the effect of normal grouting and water blocking, as shown in Figure 15a–c.

Figure 15. Overview of the shaft's engineering.

After the grouting pad on the working face cracked, two circumferential cracks and radial cracks emerged. The main circumferential crack is located approximately 2.6–3.5 m from the initial support, with a length of around 8.4 m and a width of 3.5–5.0 cm. It runs in an east–west direction, starting near the opening of the 6# grouting hole and ending at the initial support structure. The secondary crack runs parallel to the main crack and measures approximately 1.8 m in length and 2–3.0 cm in width. Radial expansion cracks are perpendicular to tangential cracks and have a lower degree of cracking than tangential cracks. The cracking of the grouting pad is shown in Figure 15d.

5.2.2. Calculation of Load Capacity of the Grouting Pad

The radius of the 2-2 shaft radius is r_2 = 5.6 m, the original design thickness of the grouting pad 2.1 m, and C25 concrete was used, with M_p = 11.5445 kN/m. There are 25 grouting holes arranged in a circular direction with a radial distance of about 1.0 m from the initial support. By substituting the lining radius r_2 = 5.6 m, c = 2.8 m, and b = 1 into Equation (8) and iteratively solving for r_1 = 4.35 m, and then substituting it into Equation (15), it can be given as:

$$q_u = \frac{(2 \times 1^2 + 6 + 8 \times 1) \times 11.5445}{(2+1) \times \left[2 \times 2.8^2 (2.8/4.35)^{1+1} - (3+1) \times 2.8^2 + 4.35^2 \times (1+1)\right]} = 4.745 \text{ MPa}$$

The water pressure of the shaft working face is 1.6 MPa, and the average injection pressure of the injection hole is 5 MPa. This means that P = 6.6 MPa < 4.745 MPa. Insufficient bearing capacity caused the punching shear failure of the 2-2 shaft grouting pad.

5.2.3. Thickness Design of the Grouting Pad

It is known that the water pressure on the working surface of the shaft is 1.6 MPa, and the average grouting pressure of the hole is 5 MPa, that is, P = 6.6 MPa, and γ is taken as 1.5. The grouting pad was poured with C40 concrete, and r_2/r_1 = 5.5/4.35 = 1.264, which is close to 1.25. Therefore, r_1 is still taken as 4.35 m, and the thickness B_0 of the grouting pad is calculated, which can be given as:

$$B_0 = \sqrt{\frac{3 \times 6.6 \times 1.5 \times (2+1)\left[2 \times 2.8^2 \times (2.8/4.35)^2 - 5 \times 2.8^2 + 4.35^2 \times 2\right]}{5.5 \times 16 \times 1.43}} = 2.87 \text{ m}$$

The actual design is 2.9 m.

Using the Chinese coal mine experience design method in Equation (12), the grouting termination pressure P_0 is taken to be 2–2.5 times the static water pressure of 3.2 MPa, and the thickness B_{01} of the grouting pad is calculated, which can be seen as:

$$B_{01} = \frac{3.2 \times 5.5}{40} + 0.3 \times 5.5 = 2.09 \text{ m}$$

Therefore, compared with the thickness of the grouting pad designed by the plastic limit method, the thickness of the grouting pad designed by the empirical calculation method of the Chinese coal mine is about less than 40%, which is consistent with the above analysis of the 2-2 shaft grouting pad due to the insufficient bearing capacity that occured through a punching shear failure.

5.3. Post-Construction Effect of the Grouting Pad

After seven days of construction and curing with C40 concrete, a series of core samples were taken at the site to perform internal uniaxial compression tests on the grouting pad. The average compressive strength of the grouting pad reached 40 MPa, indicating that the tensile strength f_t also reached the design value [31], as shown in Figure 16. After construction, the surface of the grouting pad was flat. During the grouting of the surface using the "staged, interval and hole skipping" grouting method, the problem of surface cracking of the grouting pad is well solved, as shown in Figure 17.

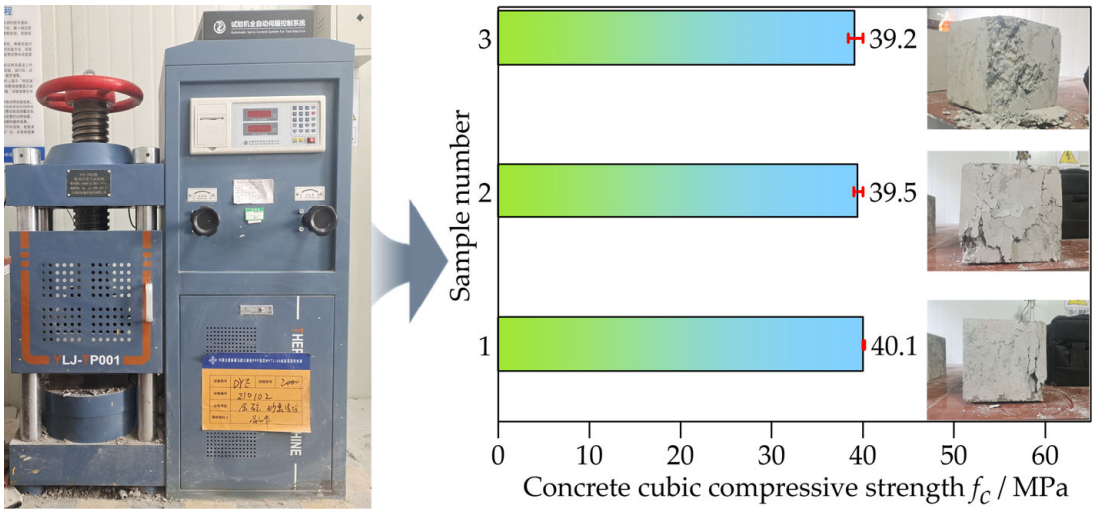

Figure 16. Concrete strength test.

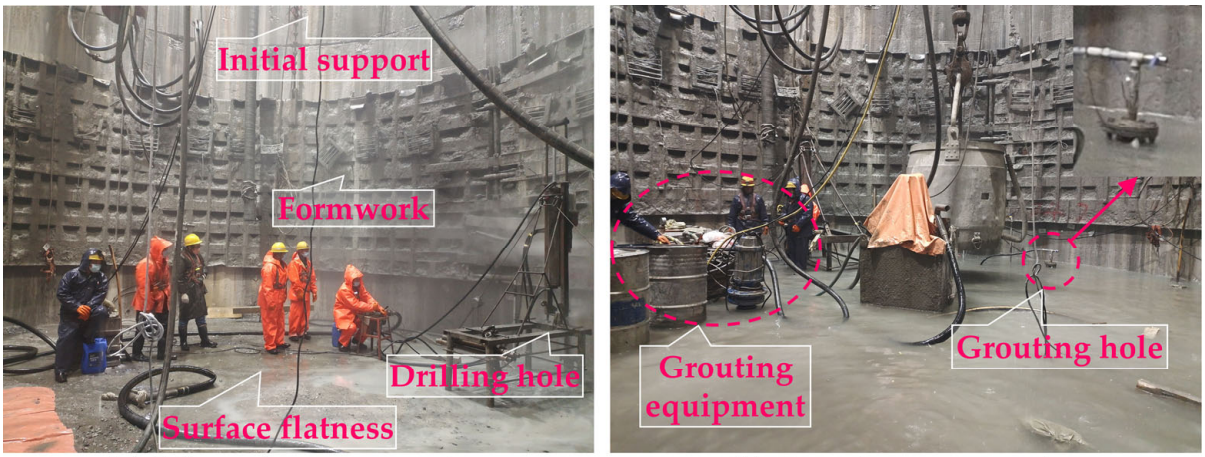

(a) Effect after construction **(b)** Grouting construction

Figure 17. The effect after the construction of the grouting pad.

5.4. Discussion

This study investigates two problems of the bearing capacity and thickness calculation of grouting pads for shafts. We have derived a unified solution for the plastic ultimate bearing capacity of grouting pads based on the analysis of the punching shear failure mode of grouting pads, considering the current lack of calculation methods for the bearing capacity of large-diameter shaft grouting pads in highway tunnels. Secondly, we propose a new plastic limit design method for grouting pad thickness in response to the problem of weak bearing capacity failure caused by previous elastic design methods for coal mine shaft grouting pads. The research results were applied to the 2-2 shaft project of the Tianshan Shengli Tunnel, which solved the problem of frequent cracking caused by the failure of the grouting pad during construction. The research findings were implemented in the Tianshan Shengli Tunnel's 2-2 shaft project, resolving the issue of frequent cracking due to grouting pad failure during construction.

Compared with existing research [32,33], this study analyses the punching shear failure mode of the grouting pad by simplifying its mechanical model as a simply supported circular plate. The grouting pressure and water pressure are equivalent to the edge load of the circular plate. The plastic structural limit analysis method is used to obtain a unified solution for the bearing capacity, which is compared with existing research. After examining the factors that influence the bearing capacity of the grouting pad, we propose a reasonable understanding that can aid in grouting construction. We clarify the bearing capacity of the grouting pad and establish a plastic limit design method for the thickness of large-diameter vertical shaft grouting pads. This method improves the defect of weak bearing capacity in the traditional elastic design method applied to the thickness design of large-diameter shaft grouting pads [29]. There are two reasons for the deviation caused by the two methods of elastic and plastic limit design. Firstly, the failure of concrete materials generally undergoes an "elastic plastic" process when failing [34]. Elastic failure occurs before plastic failure, and the required ultimate failure load is small [35]. The bearing capacity is directly proportional to the thickness B_0, according to Equation (14), so the design thickness is relatively small. Secondly, the elastic design method is based on experience and is intended for coal mine shafts with a diameter of less than 7 m. However, for highway tunnel shafts with a diameter of 7.5–10.5 m, the "diameter thickness ratio" of the grouting pad is relatively large when using the elastic design method. This poses a thin plate problem in mechanics, as thin plates are more prone to damage than thick plates.

However, the use of plastic limit analysis methods is only suitable for simple problems. The second method assumes that the material is rigid plastic and studies the behaviour of the structure when it reaches the plastic limit state based on the plastic defor-

mation law, which is also the method used in this article to calculate the capacity. Based on this study, there are two limitations:

(1) When analysing the plastic ultimate bearing capacity of the grouting pad in the paper, it is assumed that the material is rigid plastic and elastic deformation is not considered, so that the internal stress–strain distribution before the plastic ultimate state of the grouting pad cannot be obtained.

(2) When establishing the calculation model in this paper, it is assumed that the grouting pad corresponds to an axisymmetric circular plate, the bottom of the shaft working face is flat, and no settlement occurs before the grouting pad is poured. In particular, in the construction of shafts in soft rock strata, the unevenness of the working face after mucking, coupled with the influence of settlement deformation effects in soft rock strata [36,37], these result in a rather complex problem of the bearing capacity of the grouting pad, which can be further discussed in the future.

Numerical simulation methods may be used to solve the first problem mentioned above, which is the cracking problem of concrete circular plates with holes [38]. This is currently a difficult problem that computational mechanics urgently needs to overcome [39]. Traditional universal numerical calculation methods are unlikely to achieve satisfactory results. Regarding the second point, it is more complex and belongs to the category of structural rock foundation interaction problems. However, determining the load distribution characteristics can be challenging, and on-site testing methods are necessary to reveal the internal mechanism. The author's team anticipates reading reports on relevant research findings.

6. Conclusions

This paper first analyses the punching shear failure mode of a grouting pad under symmetric load. Secondly, the unified solution of the plastic limit load for grouting pad punching shear failure is deduced, and the influence law of the plastic limit bearing capacity parameter of a grouting pad is discussed; finally, the plastic limit design method of grouting pad thickness is proposed. The results of this study are applied to the optimal design of grouting pad thickness in shaft 2-2 of the Tianshan Shengli Tunnel, which solves the frequent cracking of the grouting pad. The main conclusions of this paper are as follows:

1. The grouting pad failure mode is punching shear failure. The formation of annular holes or ''weak rings'' due to peripheral grouting holes is the basic condition for failure. The bearing capacity is insufficient to withstand the lifting force produced by grouting and the water pressure on the working surface. These two factors work together to lead to punching shear failure.
2. A uniform solution for the bearing capacity of the grouting pad is derived and verified to be reasonable. When b is set to 0 and 0.5, it can degenerate to the Tresca and Mises yield criteria, respectively. The bearing capacity q_u shows a trend of first decreasing and then increasing as the value of b increases. The minimum value is reached when $b = 0.4$, and the maximum value is achieved when $b = 1$. Therefore, the unified solution is recommended for design calculations, as it better utilises the the potential of material strength.
3. When the thickness is certain, the bearing capacity of the grouting pad is inversely proportional to the ratio of the diameter to the area of the loaded area at the bottom. It is important to follow the principle of "division, interval, and hole skipping" during grouting construction. When designing a grouting pad, the maximum bearing capacity is achieved when the r_2/r_1 ratio is close to 1.25. As the ratio of r_2/c increases, the value of r_1 exhibits a three-stage trend of first decreasing, then increasing, and finally decreasing.
4. The bearing capacity of a grouting pad increases with its thickness under the same load conditions. When the diameter of the grouting pad is $2r_2$ and the thickness B_0 is constant, the bearing capacity q_u increases with an increase of the tensile strength de-

sign value f_t of the grouting pad concrete material. Following the principle of "large thickness, unified strength yield criterion, high-strength material" in the design is recommended to obtain better bearing performance of the grouting pad.

5. The new method for bearing capacity design proposed in this article has been applied in engineering practice, effectively solving the problem of frequent cracking of grouting pads during shaft grouting construction, and confirming its good feasibility and practicality. The findings have practical guidance significance for the design and construction of grouting pads for deep and large shafts of extra-long tunnels.

Author Contributions: Formal analysis and writing—original draft preparation, T.F.; resources and funding acquisition, Z.Z.; conceptualisation and methodology, J.C.; supervision and project administration, Y.L.; investigation, W.L.; validation, D.L.; writing—review and editing, R.Y.; writing—review and editing, J.L. All authors commented on previous versions of the manuscript. All authors have read and agreed to the published version of the manuscript.

Funding: This work was supported by the Key Project of the High-Speed Rail Joint Fund of the National Natural Science Foundation of China (Grant No. U2268214), National Natural Science Foundation of China (Grant No. 52308390), Natural Science Basic Research Program of Shaanxi Province (Grant No. 2023-JC-QN-0383), Scientific Research Project of CCCC First Highway Engineering Company (Grant No. X-GL-QSGS(J)-XJI-WY-05-JS-081), and Science and Technology Research and Development Project of CCCC First Highway Engineering Company (Grant YGJKT-2020-A-03).

Institutional Review Board Statement: Not applicable.

Informed Consent Statement: Not applicable.

Data Availability Statement: The original contributions presented in the study are included in the article, further inquiries can be directed to the corresponding author.

Conflicts of Interest: Author Zongzhi Zhao was employed by the company CCCC First Highway Engineering Company. Authors Dong Li, Ruibin Yu and Jian Li were employed by the company CCCC Central-South Engineering Co., Ltd. The remaining authors declare that the research was conducted in the absence of any commercial or financial relationships that could be construed as a potential conflict of interest.

References

1. Chen, J.; Liu, W.; Chen, L.; Luo, Y.; Li, Y.; Gao, H.; Zhong, D. Failure Mechanisms and Modes of Tunnels in Monoclinic and Soft-Hard Interbedded Rocks: A Case Study. *KSCE J. Civ. Eng.* **2020**, *24*, 1357–1373. [CrossRef]
2. Luo, Y.; Shi, Z.; Wang, C.; Chen, J. Mechanical properties of rock bolt and analysis for the full-process of sliding failure based on rock mass absolute displacement. *J. Traffic Transp. Eng.* **2022**, *9*, 490–506. [CrossRef]
3. Liu, W.; Chen, J.; Chen, L.; Luo, Y.; Shang, Q.; Zhang, L. A Rational Construction Method and Deformation Control System of Tunnelling in Extremely Soft and Fractured Chlorite Schist Medium. *Tunn. Undergr. Space Technol.* **2024**, *143*, 105472. [CrossRef]
4. Liu, W.; Chen, J.; Luo, Y.; Chen, L.; Zhang, L. Long-term stress monitoring and in-service durability evaluation of a large-span tunnel in squeezing rock. *Tunn. Undergr. Space Technol.* **2022**, *127*, 104611. [CrossRef]
5. Ray, R.; Fuster, E.; Lee, S. Optimizing the Performance of Vertically-Mounted Jet Fans in Ventilation Shafts. *Min. Metall. Explor.* **2022**, *39*, 927–936. [CrossRef]
6. Auvinet-Guichard, G.; Rodríguez-Rebolledo, J.F.; Rangel-Núñez, J.L. Construction of deep tunnel shafts in Mexico city soft clays by the flotation method. *Acta Geotech.* **2010**, *5*, 63–68. [CrossRef]
7. Wang, T.; Fang, B.; Hu, T.; Wei, L.; Dai, G. Field study on the application of combined grouting for the super-long drilled shaft. *Results in Engineering.* **2023**, *19*, 101366 . [CrossRef]
8. Chai, J.; Yuan, Q.; Wang, S.; Zhang, D.D.; Jiang, X.S.; Liu, F.; Sun, P.; Zhang, W.T. Management technology of vertical well flooding in Cretaceous water-bearing strata. *J. China Coal Soc.* **2016**, *41*, 338–344. [CrossRef]
9. Li, H.Y.; Wang, Q.; Jiang, B.; Zhai, S.Y.; Wang, H.P.; Li, W.T.; Li, Z. Technology of grouting and blocking water on working face with massive water in deep vertical shaft. *J. China Coal Soc.* **2011**, *36*, 444–448. [CrossRef]
10. Wang, S.Q.; Zhang, W.F.; Niu, J.S.; Liu, B. Application of grouting technology in control shaft water inrush. *Mine Constr. Technol.* **2019**, *40*, 23–26. [CrossRef]
11. Pan, R.; Zhang, B.Q. Study on design of grouting pad and rock cap at shaft sinking face above high pressurized water in mine shaft. *Coal Eng.* **2014**, *46*, 27–29. [CrossRef]
12. Q, C.; G, C. Application of Hydrostatic Slurry Pad Grouting Technology in Tianxing Iron Ore Mine 1# Sub-shaft. *Mod. Min.* **2018**, *34*, 247–251. [CrossRef]

13. Zhai, H.C.; Nan, S.Q.; Hu, W.W. Study on water treatment technologies of hydrostatic grouting pad inTianxing Iron Mine. *Ferr. Met. (Min. Compon.)* **2015**, *67*, 92–94. [CrossRef]
14. Zheng, C.M.; Ma, Z.H.; Lu, Y.G. Construction technology of grouting pad in complex hydrogeological section of vertical shaft casing. *Ind. Sci. Trib.* **2014**, *13*, 72–73. [CrossRef]
15. Öge, I.F. Prediction of cementitious grout take for a mine shaft permeation by adaptive neuro-fuzzy inference system and multiple regression. *Eng. Geol.* **2017**, *228*, 238–248. [CrossRef]
16. Hancock, S. Ventilation shaft water inflow control rossarden tin mine, Tasmania, Australia. *Mine Water Environ.* **1985**, *4*, 21–35. [CrossRef]
17. Bukowski, P. Water Hazard Assessment in Active Shafts in Upper Silesian Coal Basin Mines. *Mine Water Environ.* **2011**, *30*, 302–311. [CrossRef]
18. Han, C.H.; Xu, J.G.; Zhang, W.J.; Wei, J.C.; Yang, F.; Yin, H.Y.; Xie, D.L. Assessment and Grouting of Water Inrush Induced by Shaft-Freezing Holes in the Yingpanhao Coal Mine, Inner Mongolia, China. *Mine Water Environ.* **2022**, *41*, 16–29. [CrossRef]
19. Kipko, E.J.; Spichak, Y.u.N.; Polozov Yu, A.; Kipko, A.E.; Hepnar, P. Grouting of old flooded workings at M. Mayerova Mine in Czechoslovakia. *Mine Water Environ.* **1993**, *12*, 21–26. [CrossRef]
20. Xu, Z.P.; Feng, X.; Li, S.S.; Fan, L.M.; Liu, C.W. Simultaneous Operations of Pregrouting and Shaft Drilling in Shaft Construction. *Adv. Civ. Eng.* **2020**, *2020*, 8529236. [CrossRef]
21. Christian, C. *Mathematical Methods for Elastic Plates*, 1st ed.; Springer: London, UK, 2014; pp. 301–360. [CrossRef]
22. Pan, D.; Bu, Z.; Li, H.; Xu, Z.; Liu, J. Experimental Investigation of Flow Control Technology for Grouting and Blocking of Flowing Water in Karst Conduits. *KSCE. J. Civ. Eng.* **2022**, *26*, 3440–3454. [CrossRef]
23. Flora, A.; Modoni, G.; Lirer, S.; Croce, P.G. The diameter of single, double and triple fluid jet grouting columns: Prediction method and field trial results. *Geotechnique* **2013**, *63*, 934–945. [CrossRef]
24. Zhang, P.Y.; Zeng, B.; Ding, H.Y.; Guo, Y.H. Analysis of internal force and disengagement law for circular expansion foundation plate of onshore wind turbine. *Build. Struct.* **2020**, *50*, 129–136. [CrossRef]
25. Helmut, F.; Schweiger Kummerer, C. Numerical modeling of settlement compensation by means of fracture grouting. *Soils Found.* **2004**, *44*, 71–86. [CrossRef]
26. Theocaris, P.S. Elastic-plastic analysis of cracked plates in plane stress: An experimental study. *Acta Mech.* **1993**, *99*, 75–93. [CrossRef]
27. Yu, M.H.; Kolupaev, V.A.; Li, Y.M. Advances in Unified Strength Theory and its Generalization. *Procedia Eng.* **2011**, *10*, 2508–2513. [CrossRef]
28. Xu, B.Y.; Liu, X.S. *Plastic Limit Analysis Of Structure*, 1st ed.; China Architecture and Building Press: Beijing, China, 1985; pp. 36–75. (In Chinese)
29. Shaft Construction Engineering Manual; Cui, Y.L. *Concise Shaft Construction Manual*, 1st ed.; Coal Industry Press: Beijing, China, 2003; pp. 1325–1327. (In Chinese)
30. Bedford, A.; Liechti, K.M. *Mechanics of Materials*, 2nd ed.; Springer: Cham, Switzerland, 2020; pp. 301–360. [CrossRef]
31. Chen, Y.; Liu, L.X.; Peng, S.M. Experimental study on relationships between tensile strength and compressive strength of ready mixed concrete at different age. *Build. Struct.* **2010**, *40*, 109–111. [CrossRef]
32. Li, Z.; Lai, J.; Ren, Z.; Shi, Y.; Kong, X. Failure mechanical behaviors and prevention methods of shaft lining in China. *Eng. Fail. Anal.* **2023**, *143*, 106904. [CrossRef]
33. Li, P.; Wang, S.; Zhang, M.; Huang, Z. Supporting Structure of Steel Corrugated Plate-Mold Bag Concrete and Its Application in a Circular Shaft. *App. Sci.* **2023**, *13*, 12937. [CrossRef]
34. Marí, A.; Spinella, N.; Fernanda Rodríguez, M. Mechanical model for the shear-punching strength of steel fiber reinforced concrete slabs under concentric loading. *Structures* **2023**, *52*, 854–867. [CrossRef]
35. Ferradi, M.; Fliscounakis, A.; Arquier, M.; Bleyer, J. Elastoplastic and limit analysis of reinforced concrete with an equilibrium-based finite element formulation. *Comput. Struct.* **2023**, *286*, 107095. [CrossRef]
36. Rodríguez, C.; Rodríguez-Pérez, Á.; López, R.; Hernández-Torres, J.A.; Caparrós-Mancera, J.J. A Finite Element Method Integrated with Terzaghi's Principle to Estimate Settlement of a Building Due to Tunnel Construction. *Buildings* **2023**, *13*, 1343. [CrossRef]
37. Hu, T.; He, T.; Kang, Z.; Tu, P.; Wang, D. Establishment and engineering application of viscoelastic-plastic constitutive laws for creep modeling in interbedded rock masses. *Sci. Rep.* **2023**, *13*, 20668. [CrossRef] [PubMed]
38. Chen, J.; Hu, T.; Hu, X.; Jia, K. Study on the influence of crack depth on the safety of tunnel lining structure. *Tunn. Undergr. Space Technol.* **2024**, *143*, 104549. [CrossRef]
39. Lorefice, R.; Etse, G.; Carol, I. Viscoplastic approach for rate-dependent failure analysis of concrete joints and interfaces. *Int. J. Solids. Struct.* **2008**, *45*, 2686–2705. [CrossRef]